THE ASTROPHYSICAL JOURNAL, 366:405–411, 1991 January 10

A STRAIGHT GRAVITATIONAL IMAGE IN ABELL 2390: A STRIKING CASE OF LENSING BY A CLUSTER OF GALAXIES[1]

ROSER PELLÓ,[2] JEAN-FRANÇOIS LE BORGNE,[3] GENEVIÈVE SOUCAIL,[3] YANNICK MELLIER,[3] AND BLAI SANAHUJA[2]

Received 1990 February 26; accepted 1990 July 9

ABSTRACT

In this paper we present the results obtained on the photometry and spectroscopy of a very linear arclike object found in the center of the rich cluster of galaxies Abell 2390 ($z = 0.231$). The main feature in its spectrum is an emission line at 7130 Å that exists all along the arc. The identification of this emission line as [O II] λ3727 leads to a redshift of 0.913 for the structure. This is the third arc candidate confirmed spectroscopically as a gravitationally lensed background galaxy. We report the presence of several arclets in the neighborhood of the arc, and a faint object whose redshift and spectrum are about the same as those of the arc. We discuss the detection of a velocity gradient inside the arc. A first attempt to model the lens is also proposed, and the difficulties of reproducing a "straight arc" are emphasized.

Subject headings: galaxies: clustering — gravitational lenses

I. INTRODUCTION

During the past few years, several giant luminous arcs and faint blue gravitationally distorted images have been discovered in the center of various distant and rich clusters of galaxies (see Fort 1989*a* for a review). The redshift measurements of such structures, as in the case of Abell 370 (Soucail *et al.* 1988) and Cl 2244−02 (Soucail *et al.* 1989), have proved that they are background galaxies gravitationally distorted by the cluster core. At present, more than 10 different clusters of galaxies show an arclike structure and/or distorted images, but few of them can be confirmed spectroscopically.

In the course of an observing run with the 2.5 m Isaac Newton telescope (INT) for the Arc and Gravitationally Distorted Images Survey (1988 July), we discovered that the rich cluster Abell 2390 contains a strange linear object which, in spite of its straight shape, could be a so-called arc (Mellier 1989; Pelló *et al.* 1989). The existence of this object was confirmed one month later at the Canada-France-Hawaii 3.6 m telescope (CFHT). The peculiar geometry of such a gravitational image is difficult to explain with a simple model, so spectroscopic proof of the gravitational hypothesis was needed. Spectra of this structure and of the cluster galaxies were obtained during several runs at the CFHT, the European Southern Observatory (ESO) telescope, and the William Herschel telescope (WHT). The present paper presents the spectroscopic and photometric results on the arc and the arclets found in the center of A2390. A detailed study of the photometric and spectroscopic properties of the whole cluster obtained from the various observing runs will follow (Le Borgne *et al.* 1990), as well as a structural and dynamical analysis of the cluster (Mellier *et al.* 1990).

We present in § II the main description of the cluster. In § III we introduce the "straight arc," with a description and analysis of the photometric and spectroscopic data. The properties of the arclets in the environment of the arc are described in § IV. Finally, some preliminary results in the modeling of such structure are discussed in § V, in view of the overall observational constraints which can be included. Throughout the paper, we will assume $H_0 = 50$ km s^{-1} Mpc^{-1} and $q_0 = 0$.

II. SOME PROPERTIES OF THE CLUSTER ABELL 2390

A2390 is classified in the Abell Catalog (Abell, Corwin, and Olowin 1989) as a cluster of distance class 6 and richness class 1. Its estimated photometric redshift is 0.195 (Kowalski *et al.* 1984), and it belongs to the Rood and Sastry class LA (Struble and Rood 1987). The cluster is dominated by a large cD galaxy in its center. Owen *et al.* (1982) have detected an elongated radio source at 1400 MHz close to the center of the cluster (0.35 ± 0.09 Jy). A2390 is also a strong X-ray emitter. The total X-ray luminosity is 9.77×10^{44} ergs s^{-1} in the range 2–6 keV ($H_0 = 75$ km s^{-1} Mpc^{-1}) (Kowalski *et al.* 1984) and 4.67×10^{44} ergs s^{-1} in the range 0.7–3.5 keV (Ulmer, Kowalski, and Cruddace 1986). *Einstein Observatory* X-ray maps may be found in Ulmer, Kowalski, and Cruddace (1986) and in McMillan, Kowalski, and Ulmer (1989).

The first CCD images of the cluster were taken at the prime focus of the INT, using an RCA2 CCD with a pixel size of 0ʺ74. The size of the whole CCD field is 4ʹ0 × 6ʹ3. The seeing conditions ranged from 1ʺ to 1ʺ3. Five frames were obtained using the g and r filters of the Thuan-Gunn system (Thuan and Gunn 1976) and B_J (Johnson system), with exposure times of 2 × 1800 s in r, 2100 s in g, and 2 × 2700 s in B_J. The second set of deep images of the central part of the cluster (2ʹ2 × 3ʹ5) was obtained at the prime focus of the 3.6 m CFHT, with a higher resolution and sampling: 0ʺ205 pixel^{-1} and seeing of about 0ʺ7. Six frames were taken using Bessel filters B and R, with exposure times of 3 × 1800 s in B and 3 × 900 s in R. From both sets of CCD frames, we performed the photometry of the whole cluster and of a comparison field, and determined their main properties (Le Borgne *et al.* 1990). The concentration index and N_{30}, which follow the definition by Butcher and Oemler (1984), are $C = 0.37$ and $N_{30} = 36$, respectively. The

[1] Based on observations made with the Isaac Newton and William Herschel telescopes operated on the island of La Palma by the Royal Greenwich Observatory in the Spanish Observatorio del Roque de Los Muchachos of the Instituto de Astrofísica de Canarias, the 3.6 m telescope at the European Southern Observatory (La Silla, Chile), and the Canada-France-Hawaii 3.6 m telescope.

[2] Departament de Física de l'Atmosfera, Astronomia i Astrofísica, and Grup d'Astrofísica del Institut d'Estudis Catalans, Universitat de Barcelona, Spain.

[3] Observatoire Midi-Pyrénées, Toulouse, France.

orientation (133°.3) and ellipticity (0.202) of the X-ray image (McMillan, Kowalski, and Ulmer 1989) closely follow those of the isoluminosity and isodensity contour plots for the galaxies belonging to the cluster. The orientation of the cluster is about $133° \pm 15°$, with an ellipticity of about 0.29 (all the position angles in this paper are counted counterclockwise from north to east). The spectra of the cluster galaxies obtained during the different observing runs lead to a mean redshift of 0.231 for the cluster.

III. THE STRAIGHT ARC

a) *Morphology and Photometry*

Both sets of CCD images show that this structure has a rectangular shape, 15″ long and 1″.3 wide. It is well resolved on the CFHT images. It is located 37″ northwest from the central galaxy, and the closest galaxy lies 3″ away from the arc. This galaxy has a redshift $z = 0.231$, so it belongs to the cluster. On the arc, there are two breaks, symmetrically located with respect to the center of the close galaxy, as shown in Figure 1 (Plate 7). So this "straight arc" is divided into three regions, 3″.0, 5″.6, and 6″.4 long. The location of the two breaks with respect to the center of the galaxy is exactly symmetric, at least within 1 CFHT pixel. The orientation of the arc is $28° \pm 3°$. The deviation from a perfect straight line is less than 1 CFHT pixel between the two edges, so the curvature radius is larger than 9′. The total length of the arc at the redshift of the cluster is 76 kpc.

The total magnitude of the arc is $B = 21.9 \pm 0.1$. The surface brightness is variable along the structure, but, within the errors, the color indices are constant. There are two zones of brightness enhancement, symmetric with respect to the closest galaxy: one in region A, close to the first break, and one in region C, close to the second break. The mean B surface brightness is roughly 25.3 mag arcsec^{-2}, and it is about 23.4 mag arcsec^{-2} in R. The values for the color indices compared with the mean values for the cluster galaxies (in parentheses) are the following (± 0.1 mag):

$$B_J - g = 1.01 \quad (0.9)\,,$$
$$g - r = 0.59 \quad (1.3)\,,$$
$$B - R = 1.93 \quad (2.5)\,.$$

Therefore, the color indices of the arc correspond to an object significantly bluer than the galaxies in the cluster, especially for the $g - r$ index, but redder than the other known giant arcs. The giant arc in A370 shows $B - R \simeq 1.3$ (Soucail *et al.* 1987). In the case of Cl 2244−02, the mean value of $B - R = 1.11$ (Hammer *et al.* 1989).

b) *Spectroscopy of the Arc*

i) *Observations and Reduction Procedures*

Spectra of the arclike structure were obtained during three runs at the ESO 3.6 m telescope (1988 October and 1989 October) and at the 4.2 m WHT (1989 August).

Spectra were obtained at ESO in 1988 using the ESO faint object spectrograph and camera (EFOSC) system in the long-slit configuration, with a spectral range between 4000 and 7000 Å. However, the spectra of the arc did not show any strong feature to determine its redshift. This was only possible by means of the red spectra obtained during the WHT and ESO runs in 1989.

The WHT spectra were obtained using the faint object spectrograph (FOS) in the long-slit configuration (2″ × 3′). The spectrograph was set on the first-order red mode, with a spectral coverage of 4700–9800 Å and a spectral resolution of 22.3 Å. The detector was a GEC CCD (10 e^- rms), with a pixel of 8.9 Å × 0″.67. The wavelength calibration was done using the spectra of a Cu-Ar arc lamp. The exposures on the arc were 1 hr each, taken with the slit aligned on the structure. The total exposure time was 15 hr with seeing ranging between 0″.8 and 1″.5. All the individual spectra were calibrated in flux with the star G138-31 (Filippenko and Greenstein 1984).

During the ESO run in 1989, one medium-resolution spectrum of the arc was taken using EFOSC and the R150 grism. The spectral coverage was 6800–8700 Å. The detector was a CCD RCA2, with a pixel of about 3.6 Å × 0″.67. A long slit 1″.5 wide was used. The exposure time was 1 hr, and the seeing conditions about 1″.4.

From each of the 15 WHT spectra we extracted a zone of 42″ (63 pixels), centered on the arc, and a mean sky spectrum. The mean sky frames were subtracted from each column of these spectra, in order to construct 15 two-dimensional sky-corrected images. A final two-dimensional clean spectrum was obtained by recentering the frames and computing the median of each pixel over all the frames (Fig. 2 [Pl. 8]). Re-centering was done using the three galaxies close to the arc as seen in Figure 2. A standard procedure was used to correct the ESO medium-resolution spectrum. In all the cases, we used standard wavelength and flux calibrations, as well as flat-field corrections.

ii) *Main Properties of the Spectrum*

Each one of the 15 WHT spectra of the arc shows an emission line at 7130 Å, which is present all along the arc. The spectrum obtained at ESO, with better resolution but a lower signal-to-noise (S/N) ratio, shows the same characteristics. Since the S/N ratio is reasonably good in the WHT median spectrum, we used this to produce the spectra of the three main parts of the arc separated by the two breaks mentioned above: region A is the southern part of the arc, region B is the middle part, and region C is the northern part. The general shape of the continuum seems to be the same in all three regions, although region B shows some contamination from the nearby galaxy, and it is in good agreement with the color indices. When we use the 15 co-added spectra of the arc instead of the median spectrum, the contamination due to the nearby galaxy becomes evident. The shape of the continuum is mainly that of the galaxy, and some strong absorption features can be identified, such as Mg I (Fraunhofer b line), Hβ, and the Fraunhofer G band. This effect is due to the strong contamination present on some exposures, and it can be avoided by using the median spectrum because the exposures with only a slight contamination dominate the statistics.

If we identify the emission line, the main feature in the spectrum, as [O II] λ3727, the redshift is 0.913. The spectra of the three regions are compared in Figure 3 with a synthetic spectrum of a nonevolved Im galaxy redshifted at $z = 0.91$ (Rocca-Volmerange and Guiderdoni 1988). In general, the spectra of the arc are in good agreement with an Sd or Im synthetic spectrum, even though the S/N ratio is very low for $\lambda > 7500$ Å because of the strong sky features. The identification of the emission line is consistent with the shape of the continuum, which is very flat, and the satisfactory fit by the synthetic spectrum. Furthermore, other lines may be identified with this redshift, such as Mg II λ2802. Even though the S/N is poor for

1991ApJ...366..405P

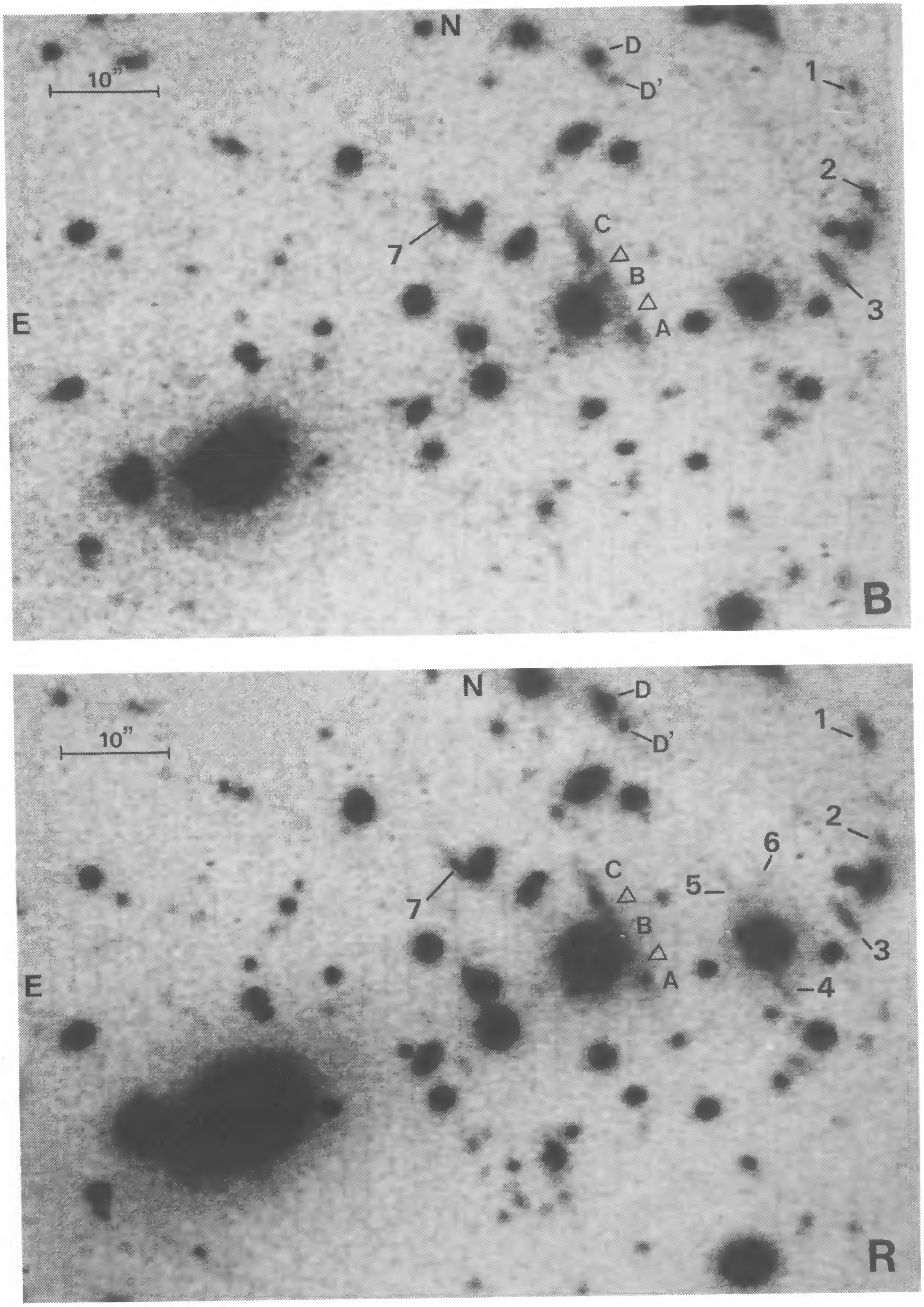

FIG. 1.—Bessel *B* (*top*) and *R* (*bottom*) CCD images of the arc and its surrounding region. These images were obtained at the Canada-France-Hawaii 3.6 m telescope (prime focus). The faint and elongated objects (arclets) are identified (see text and Table 1).

PELLÓ *et al.* (*see* **366**, 406)

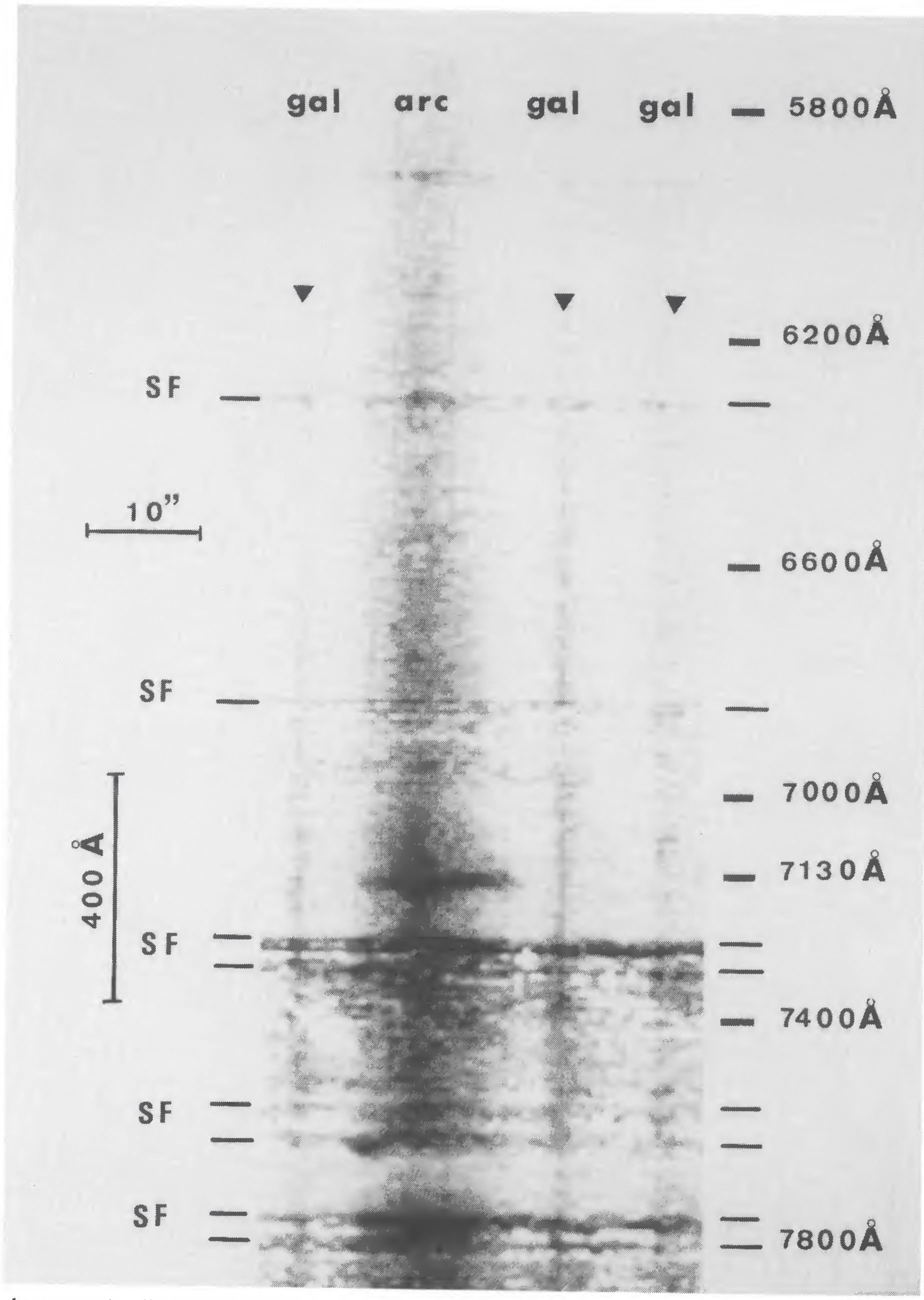

FIG. 2.—Two-dimensional spectrum (median of 15 individual spectra) of the arc and three neighboring objects, showing the 7130 Å emission line all along the arc. Blue is at the top.

PELLÓ *et al.* (*see* **366**, 406)

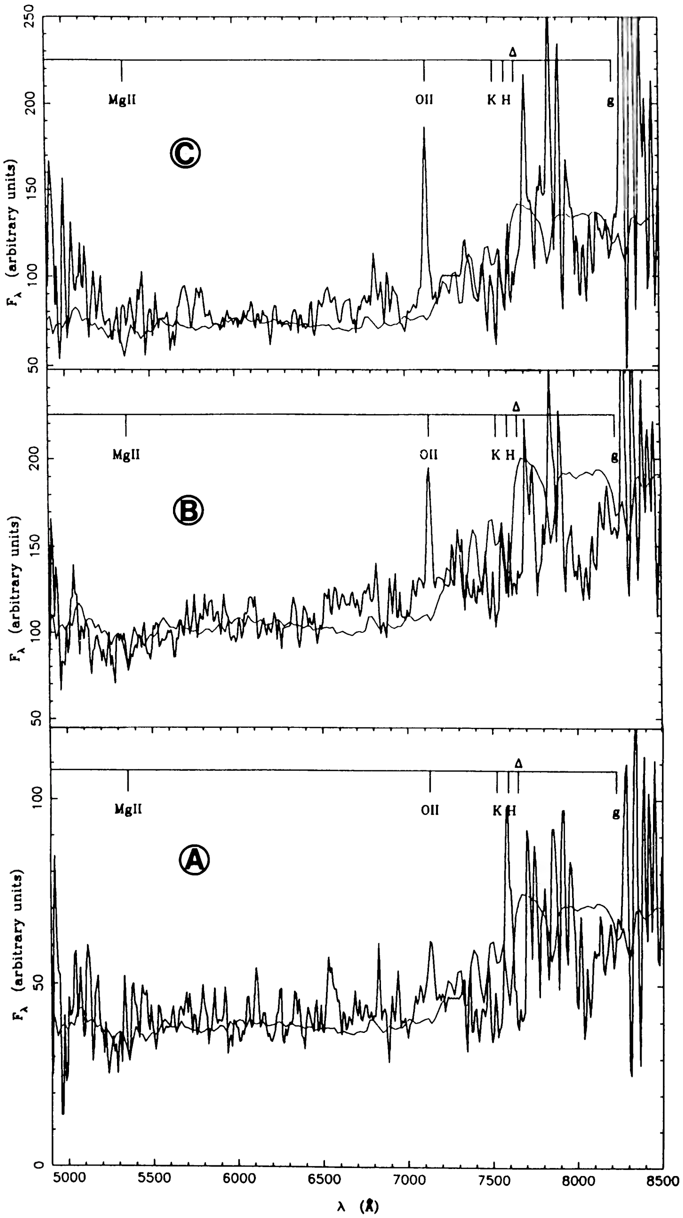

FIG. 3.—Spectra of the arc regions, from A (*bottom*) to C (*top*), compared with a synthetic spectrum of a nonevolved Im galaxy redshifted at $z = 0.91$ (*thin lines*). Each of the spectra is the sum of the columns corresponding to a given region in the two dimensional mean spectrum. The scales in F_λ are in arbitrary units. Different spectral features are identified. The continuum of the synthetic spectra has been normalized in order to fit the observed continua in the range 6000–6500 Å.

$\lambda > 7500$ Å, the continuum level of the sky-free spectral intervals after 7500 Å is higher than before. The ratio between the two flux levels after and before 7500 Å is about 2.3. This difference is compatible with a 4000 Å discontinuity at $z = 0.913$ (7650 Å), but the flux level in the red side of the spectrum is lower than predicted by the nonevolved synthetic spectra. No strong absorption lines are expected in the blue side of the spectrum between 5500 and 7000 Å.

What is striking on both WHT and ESO two-dimensional spectra (Fig. 2) is that the central wavelength of the emission line is slightly variable along the arc: it is bluer in region C than in region B. This wavelength is plotted in Figure 4. Each point is the mean value of the wavelength determination on a single pixel of the arc over all the 15 WHT spectra, and the error bars represent $\pm 1\ \sigma$ intervals. All of the 15 WHT spectra show the same shift in the emission-line wavelength along the arc, within 2 σ. This phenomenon is also confirmed independently by the ESO spectrum (Fig. 4), even though several pixels in the range 18–23 are lost owing to CCD defects. There is a slight constant shift in the ESO wavelength values with respect to the WHT values, and it is probably due to the relative uncertainties in the wavelength origin, mainly because of the difference in resolution between the two sets of spectra. The mean value (± 2 Å) of the line wavelength slowly changes from about 7134 Å in region A to 7129 Å in region C, being about 7138 Å in region B. The difference of 9 Å between the two extreme values can be translated into a velocity difference of 378 km s^{-1} between the two regions. Further comments on this will be given in § VI.

The energy flux above the continuum level within the emission line is almost constant between pixels 6 and 23 (regions B and C). Between pixels 1 and 5 (region A) the energy flux is also constant, but its value is only about 75% of the mean level in regions B and C.

IV. PROPERTIES OF THE "ARCLETS" NEAR THE ARC

Near the arc, in the same region of the cluster, there are several faint elongated objects whose orientation is roughly the same as that of the arc. In fact, all the faint and elongated objects in this region seem to be parallel to this orientation, and perpendicular to the major axis of the isodensity contour plot, with $\pm 10°$. These faint objects may be considered as the so-called arclets, often associated with rich clusters (Fort *et al.* 1988). The photometric properties of this population are summarized in Table 1, where the identification numbers refer to Figure 1. Successive columns are as follows: (1) identification number; (2, 3) total Bessel *B*- and *R*-magnitudes; (4) $B-R$; (5, 6) *B* and *R* surface brightness of the central pixel, in mag arcsec^{-2}; (7) size of the major axis in arcseconds; (8) orientation of the major axis; and (9) orientation difference with

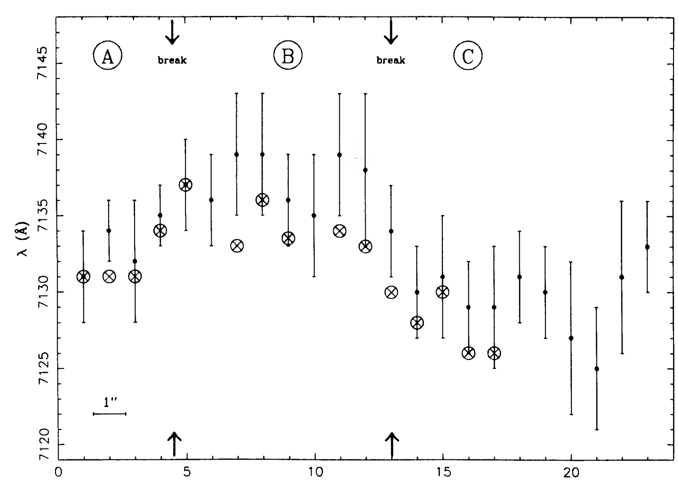

FIG. 4.—Position of the emission-line center along the arc, as obtained from the 15 WHT spectra. The error bars correspond to 1 σ. The origin on the abscissa is taken from the first pixel in region A, and the position of the breaks is indicated by arrows. The result coming from the ESO spectrum are plotted as circled crosses.

TABLE 1

MAIN PHOTOMETRIC PROPERTIES OF FAINT ELONGATED OBJECTS IN NEIGHBORHOOD OF ARC

Object (1)	Bessel B (2)	Bessel R (3)	Bessel $B-R$ (4)	μ_B (mag arcsec^{-2}) (5)	μ_R (mag arcsec^{-2}) (6)	Major-Axis Size (7)	ϑ (8)	$\vartheta-\vartheta_{arc}$ (9)
1..............	25.05	22.35	2.70	26.0	23.4	3."6	28°	0°
2..............	23.85	22.66	1.19	25.0	24.7	3.6	40	+12
3..............	23.65	21.97	1.68	25.6	23.7	5.3	42	+14
4..............	25.37	22.17	3.20	>27.0	24.4	4.6	36	+8
5..............	25.80	22.43	3.37	>27.0	24.4	5.3	32	+4
6..............	24.91	22.53	2.38	>27.0	24.3	4.7	15	−13
7..............	23.43	22.07	1.36	24.8	23.4	3.6	33	+5

respect to the arc. In general, the photometric properties of the arclets, such as surface brightness and colors, are not similar to those of the arc.

We do not have any spectra of these arclets. However, there is another faint and slightly elongated object, close to the arc, with exactly the same redshift as the arc and a similar spectrum. When fitted with an ellipse, the eccentricity of its CFHT R image is equal to 0.70: 82% of the objects of comparable magnitude (in a range of ± 0.8 mag) are less elongated. This object is identified by D in Figure 1, and its spectrum, obtained at the WHT with 1800 s of exposure, is shown in Figure 5. There is a strong emission line at 7129 Å, again identified with the 3727 Å [O II] line, leading to a redshift of $z = 0.913$. The continuum is roughly the same as that of the arc, but the shape of the spectrum is well matched by the nonevolved synthetic spectrum of an Sc galaxy, whereas the arc seems to show a slight depression on the red side of the spectrum. This is the only case of similarity to the arc among the sample of 86 objects for which we have spectra. The total B-magnitude of object D is 23.28, with $B_J - g = 1.07$, $g - r = 0.76$, and $B - R = 1.90$. Then, the color indices are roughly the same as those of the arc, but slightly redder in the $g - r$ index, and the surface brightness is higher, being 22.95 mag arcsec^{-2} in R. The object D′, which is very close to D, is fainter and redder than D, with a total B-magnitude of 24.39 and $B - R = 2.27$. It does not seem to be related to D.

Finally, looking carefully at the CCD frames, one can notice the presence of very faint and elongated structures on the opposite side of the cD galaxy (see Fig. 1). However, they are just marginally detected, and deeper frames are needed to confirm their existence.

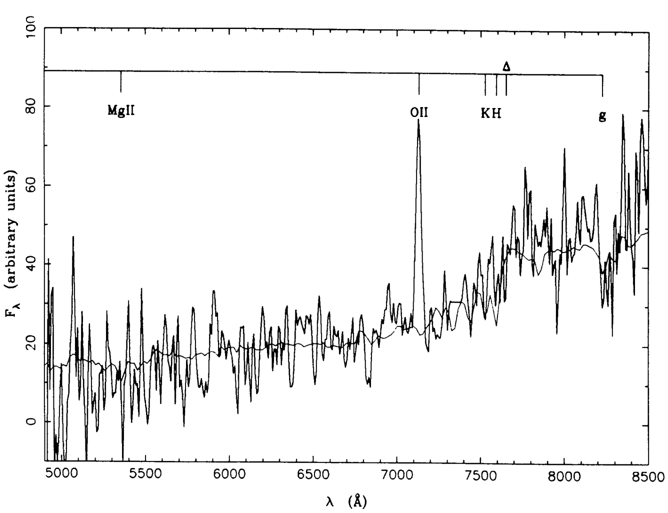

FIG. 5.—Spectrum of object D, showing the same features as the spectrum of the arc.

V. AN ATTEMPT TO MODEL THE ARC

a) Basic Assumptions

The models proposed here were obtained using a modified version of the code developed by Kovner (1987, 1989). The fit of the different parameters to the observational data is performed with a Monte Carlo sorting of the parameters within a realistic range. The two-dimensional potential used in the models is a superposition of several individual components, each of them assumed to be a distorted pseudoisothermal elliptical model:

$$\Phi(x, y) = f[b^2 + x^2(1 - \epsilon) + y^2(1 + \epsilon)]^{1/2} ,$$

with

$$f = 4\pi(\sigma/c)^2(D_{ls}/D_{os}) ,$$

where b, ϵ, and σ are, respectively, the core radius, the ellipticity, and the line-of-sight velocity dispersion of the cluster. D_{ij} is the angular diameter distance from i to j (Weinberg 1971), and the subscripts l, o, and s identify, respectively, the lens, the observer, and the source.

Taking into account the general shape of the cluster, as it can be derived from the isodensity and isoluminosity contour plots, it is assumed that the cluster is dominated by a main potential centered on the bright radio galaxy. Two classes of configurations for the potentials are investigated. The first one (Fig. 6) includes a small potential near the arc, and the shape of the source corresponds to a spiral galaxy. This assumption is used in order to reproduce the two breaks along the arc. In the second case (Fig. 7), the source is elliptical. In order to obtain a nice straight arc, a second potential is needed on the opposite side.

The overall size of the source fitted by the code is about 1″ in all the cases, a typical value for a galaxy at $z = 0.9$. The total mass located inside the volume defined by the distance from the arc to the cluster center (i.e., 37″) is $(2 \pm 0.5) \times 10^{14}\ M_\odot$. This value can be easily derived assuming that the arc is located on the Einstein radius R_E of a spherical potential:

$$M = \frac{c^2}{4\pi G} \frac{D_{os}}{D_{ol} D_{ls}} R_E^2 .$$

b) Results

The velocity gradient observed along the arc strongly supports the assumption of a spiral galaxy for the source. In model 1 the orientation and eccentricity of the main potential well are

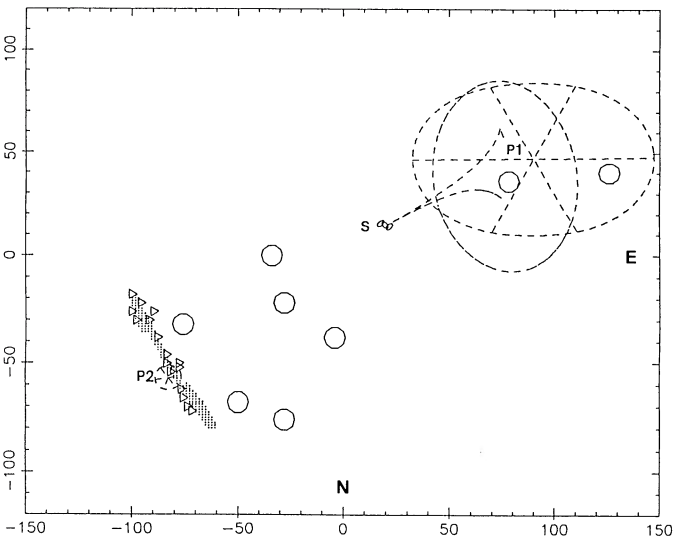

FIG. 6.—Results obtained from model 1. S indicates the position of the source. The shaded area is the resulting arc, and the small triangles match the shape of the observed arc. The positions of the bright galaxies are represented by circles. Dashed lines show the potentials (P1 and P2) and the caustic lines of the source plane.

taken as free parameters. The line-of-sight velocity dispersion found for the main potential is 1250 km s^{-1}. As shown in Figure 6, the resulting image is a straight object composed by three substructures. This image is roughly similar to the arc, but it is too thin and too long. It should be possible to fit the shape of the arc better with an arbitrary choice of a thicker bulge and shorter spiral arms. But even in this case, the results are not fully satisfactory. The orientation of the potential needed to match the shape and the position of the arc does not follow the orientation of the cluster (defined both by the optical isopleth and the X-ray isophotes). Besides, another small potential is needed, and it has to be located on the arc itself, instead of on the close galaxy, in order to avoid any curvature on the arc. Therefore, it does not correspond to the location of any visible mass. In addition, though the model produces two discontinuities at the junction of the arms with the bulge, it is unable to reproduce two breaks.

In the second model, the orientation of the total potential is forced to match the orientation of the isopleth map, with a position angle of about 133°. In principle, it is possible to obtain a straight arc if the source is located exactly on the cusp caustics. In such a cusp catastrophe, the three subarcs correspond to three merging images of the source, as shown in Figure 9 of Blandford and Narayan (1986). But in that case the three images are strongly distorted and elongated, and it is nearly impossible to reproduce the correct shape with a source of 1″. The alternative is to locate the source outside the cusp (single-image configuration) and to reproduce a straight arc by adding a secondary massive potential on the opposite side of the image (Fig. 7). Although the source is assumed to be elliptical, it can be consistent with the velocity gradient if one considers it as an edge-on spiral. The main advantage of this class of models is that it creates a saddle region in the global potential well near the arc, which can easily explain why we observe several parallel arclets only in this side of the central galaxy. The presence of a secondary potential is supported by the isoluminosity map for the cluster galaxies, which presents an enhancement 2′ northwest from the central galaxy, following the orientation of the cluster (Fig. 8). The maximum value of the secondary peak is about one-half the brightness for the main clump created by the central galaxy. Most of the bright galaxies that contribute to this secondary enhancement belong to the cluster (Le Borgne *et al.* 1990). Figure 8 shows the r isoluminosity map for the galaxies with $B_J - r > 1.8$, which mainly correspond to the E/S0 galaxies in the cluster. The problem is that the mass needed for the secondary potential at such a distance from the arc is about the same as the mass involved in the main potential. The alternative is to locate a less important potential closer to the arc, as shown in Figure 7. The problem in this case is that it does not correspond to a visible mass excess. Could it be preliminary evidence for the presence of clumps of dark matter inside the clusters of gal-

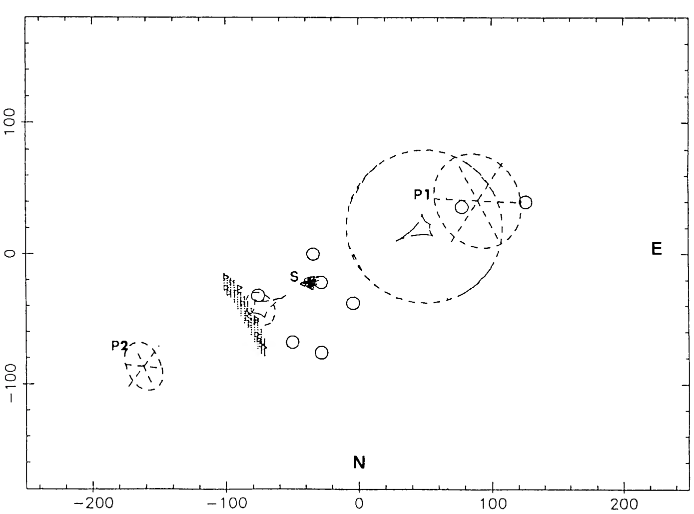

FIG. 7.—Results obtained from model 2. The symbols used are the same as in Fig. 6.

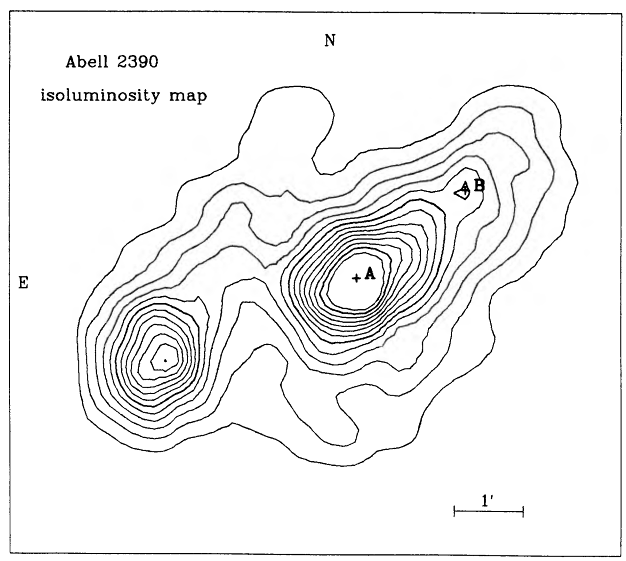

FIG. 8.—Isoluminosity map of A2390 (filter r). Only galaxies with $B_J - r > 1.8$ are used (mainly E/S0 galaxies belonging to the cluster) on a 6′.3 × 6′.3 field. The clump created by the central galaxy and the secondary clump in the northwest direction are identified as A and B, respectively.

axies, or is it possible that this secondary potential is associated with a more distant cluster or group of galaxies? In any case, deep CCD images several arcminutes away from the cluster center in that direction should give important information about this problem.

Another point about model 2 is that the straight arc in Figure 7 does not show any break. Nevertheless, this problem could be partly solved if we consider that the source is a compact pair or group of interacting galaxies. It is easy to fit such a group by an elliptically shaped source, without major constraints, in the same way as it is possible to fit an edge-on spiral galaxy. The existence of a group of galaxies at $z = 0.9$ could also explain the location of the arclets in this particular place, and the presence of object D near the arc supports this point. But this explanation is not very satisfactory because of all the " ad hoc " hypothesis involved.

Finally, the high symmetry of the two breaks with respect to the center of the nearby galaxy may be due to a direct gravitational effect of the galaxy upon the arc. In this case, no discontinuities are needed in the source in order to produce the breaks. This eventuality should be checked, since it could give information on the mass of the galaxy. At the present stage, however, the parameters in the models are not constrained enough to allow such an investigation.

VI. DISCUSSION AND CONCLUSIONS

Concerning this "straight" arc, the results show that its spectrum corresponds to a $z = 0.913$ background galaxy, probably a late-type one with active star formation. In spite of its surprising abnormal shape when compared with other known arcs, it is hard to explain the size and the photometric properties of this structure without arguing in terms of gravitational lensing.

The observed shift of the emission-line wavelength along the arc, translated into a velocity difference of 378 km s^{-1}, is compatible with a typical rotation velocity for a disk galaxy. However, this velocity is compatible with the rotation velocity of an Sc or earlier type spiral (Rubin, Whitmore, and Ford 1988) rather than with an Sd or Im type as suggested by the spectral energy distribution of the spectrum. But one must keep in mind that the observed spectrum well fits a synthetic *unevolved* Sd-Im spectrum and that an earlier type spiral at $z = 0.9$ may have a similar spectrum. Then the source of the lens may be a nearly edge-on galaxy. The regions B and C of the arc could be respectively the images of the redshifted and blueshifted parts of the disk. Another possibility for the source is a very compact group of interacting galaxies. If the properties of the emission line change all along the arc, it means that the arc is most probably a single image of the source, with a very large distortion factor. Moreover, the two breaks are exactly symmetrically located with respect to the center of the nearby galaxy, and they separate regions of different behavior. The two enhancements on the surface brightness of the arc are also symmetric with respect to the galaxy. These symmetries may be due to a gravitational effect of the galaxy upon the arc.

The arc is nearly perpendicular to the major axis of both the X-ray map and the isoluminosity contour plot. Furthermore, in the same region of the cluster, there are several faint elongated objects (arclets) whose orientations are roughly the same as that of the arc. Their surface brightness is similar to that of the arc in most cases, but they show a variety of color indices ranging from $B-R = 1.19$ to 3.37, and objects 4–6 are clearly fainter than the arc. As mentioned in § IV, these arclets are often associated with rich clusters, and they may be explained as a lensing effect on the Tyson's population of galaxies by the cluster (Tyson 1988; Fort 1989*a*, *b*). The efficiency of the lens strongly depends on the shape of the projected cluster potential. The presence of this population of arclets in this particular place points out the existence of peculiar conditions in the potential and/or background sources (clumping) which favor the formation of such gravitationally distorted images, and it is important in order to constrain the models.

We propose two ways of explaining the shape and the main properties of the arc which lead to different suggestions for the total mass distribution in the cluster. In the first model, a single image of a spiral galaxy is obtained, with two discontinuities, in good agreement with the data. The main problem with this model is the orientation of the cluster potential, which does not follow the X-ray and optical cluster profiles. The second model introduces a bimodal potential, and this configuration can explain the presence of a population of arclets in the neighborhood of the arc. The secondary potential is consistent with the optical isoluminosity map for the cluster galaxies, which shows a slight excess 2′ northwest from the central galaxy. However, the mass needed in the secondary potential, at such a distance, is too large compared with the mass involved in the main potential. The formation of a straight arc by merging three images seems to be in contradiction to the spectrum of the arc, which points to a single image. In any case, neither of the two models proposed is fully satisfactory, but both of them manage to explain several of the observed characteristics. It should be noted that nowhere in the literature was the formation of such an image predicted. More work is still needed in order to investigate this fascinating configuration thoroughly.

The presence of object D, exactly at the same redshift as the arc but with a slightly different spectrum, could be explained as another image of the same background galaxy. In any case, object D and the lensed background galaxy are in the same source plane, and all the realistic models that propose to explain the configuration of the arc will have to take into account the fact that it is weakly distorted.

The main properties of the arc lead us to the conclusion that this is a new case of a gravitational lens produced by the cluster core on a background field galaxy. In the present case we have a great deal of information concerning the cluster and the arc itself, and all this information may strongly constrain the models. However, because of the complexity of the data and the high number of constraints, the explanation of all the characteristics of the structure becomes a difficult challenge. This straight arc remains an exotic object. Its study will probably lead to a better understanding of the dark matter distribution in the cluster.

We would like to thank M. Breare, M. Cailloux, B. Fort, G. Mathez, and J.-P. Picat for their comments and help during the observations and the data reduction. Our thanks to I. Kovner (Weismann Institute) for providing a first version of his code to model the arcs. We are also very grateful to R. Blandford and C. Kochanek. We appreciated very much the discussions we had with all of them about this subject. This work has been supported by URA 285 of the Centre National de la Recherche Scientifique, associated with the Université Paul-Sabatier; by the Spanish CAICYT grants 4008-84 and 292-86; and by a fellowship from the Erasmus program.

REFERENCES

Abell, G. O., Corwin, H. G., and Olowin, R. P. 1989, *Ap. J. Suppl.*, **70**, 1.
Blandford, R. D., and Narayan, R. 1986, *Ap. J.*, **310**, 568.
Butcher, H., and Oemler, A., Jr. 1984, *Ap. J.*, **285**, 426.
Filippenko, A. V., and Greenstein, J. L. 1984, *Pub. A.S.P.*, **96**, 530.
Fort, B. 1989*a*, in *Proc. 12th Internat. Conf. on General Relativity and Gravitation* (Boulder) (Cambridge: Cambridge University Press), in press.
———. 1989*b*, in *Proc. Toulouse Workshop on Gravitational Lensing*, ed. Y. Mellier, B. Fort, and G. Soucail (Berlin: Springer), p. 221.
Fort, B., Prieur, J. L., Mathez, G., Mellier, Y., and Soucail, G. 1988, *Astr. Ap.*, **200**, L17.
Hammer, F., Le Fèvre, O., Jones, J., Rigaut, F., and Soucail, G. 1989, *Astr. Ap.*, **208**, L8.
Kovner, I. 1987, *Ap. J.*, **321**, 686.
———. 1989, *Ap. J.*, **337**, 621.
Kowalski, M. P., Ulmer, M. P., Cruddace, R. G., and Wood, K. S. 1984, *Ap. J. Suppl.*, **56**, 403.
Le Borgne, J. F., Mathez, G., Mellier, Y., Pelló, R., Sanahuja, B., and Soucail, G. 1990, *Astr. Ap. Suppl.*, in press.
McMillan, S. L. W., Kowalski, M. P., and Ulmer, M. P. 1989, *Ap. J. Suppl.*, **70**, 723.
Mellier, Y. 1989, in *Clusters of Galaxies*, ed. M. Fitchett (Baltimore: Space Telescope Science Institute).
Mellier, Y., Mathez, G., Soucail, G., Le Borgne, J. F., Fort, B., and Pelló, R. 1990, in preparation.
Owen, F. N., White, R. A., Hilldrup, K. C., and Hanisch, R. J. 1982, *A.J.*, **87**, 1083.
Pelló, R., Le Borgne, J. F., Mathez, G., Mellier, Y., Sanahuja, B., and Soucail, G. 1989, in *Proc. Toulouse Workshop on Gravitational Lensing*, ed. Y. Mellier, B. Fort, and G. Soucail (Berlin: Springer), p. 293.
Rocca-Volmerange, B., and Guiderdoni, B. 1988, *Astr. Ap. Suppl.*, **75**, 93.
Rubin, V. C., Whitmore, B. C., and Ford, W. K., Jr. 1988, *Ap. J.*, **333**, 522.
Soucail, G., Mellier, Y., Fort, B., Hammer, F., and Mathez, G. 1987, *Astr. Ap.*, **184**, L7.
Soucail, G., Mellier, Y., Fort, B., Mathez, G., and Cailloux, M. 1988, *Astr. Ap.*, **191**, L19.
———. 1989, in *Proc. Toulouse Workshop on Gravitational Lensing*, ed. Y. Mellier, B. Fort, and G. Soucail (Berlin: Springer), p. 291.
Struble, M. F., and Rood, H. J. 1987, *Ap. J. Suppl.*, **63**, 555.
Thuan, T. X., and Gunn, J. E. 1976, *Pub. A.S.P.*, **88**, 543.
Tyson, J. A. 1988, *A.J.*, **96**, 1.
Ulmer, M. P., Kowalski, M. P., and Cruddace, R. G. 1986, *Ap. J.*, **303**, 162.
Weinberg, S. 1971, *Gravitation and Cosmology* (New York: Wiley).

JEAN-FRANÇOIS LE BORGNE, YANNICK MELLIER, and GENEVIÈVE SOUCAIL: Observatoire Midi-Pyrénées, 14 Avenue Edouard-Berlin, F-31400 Toulouse, France

ROSER PELLÓ and BLAI SANAHUJA: Departament de Física de l'Atmosfera, Astronomia i Astrofísica, and Grup d'Astrofísica del IEC, Facultat de Física, Universitat de Barcelona, Diagonal, 647, E-08028 Barcelona, Spain